Effect of neodymium (Nd) doping on the photocatalytic organic dye degradation performance of sol-gel synthesized $CoFe_2O_4$ self-assembled microstructures

S. Hemasankari,[a] S. Priyadharshini,[b] D. Thangaraju,[b*] V. Sathiyanarayanamoorthi[a*], Njod Mansour Hasan Alsdran[c], Mohd. Shkir*[c,d]

[a]*Department of Physics, PSG College of Arts and Science, Coimbatore-641014, Tamil Nadu, India*

[b]*nano-crystal Design and Application Lab (n-DAL), Department of Physics, PSG Institute of Technology and Applied Research, Coimbatore-641062, Tamil Nadu, India.*

[c]*Department of Physics, Faculty of Science, King Khalid University, Abha 61413, Saudi Arabia.*

[d]*Department of Chemistry and University Centre for Research & Development, Chandigarh University, Mohali 140413, Punjab, India.*

Corresponding author

dthangaraju@gmail.com(Thangaraju Dheivasigamani)

(sathyanarayanamoorthy@yahoo.co.in) V. Sathyanarayanamoorthi

Submitting author*

shkirphysics@gmail.com

Abstract

Trivalent Neodymium doped $CoFe_2O_4$ was investigated as the potent photocatalyst for wastewater treatment. The $CoFe_2O_4$ and Nd-doped $CoFe_2O_4$ with various concentrations, such as 5, 10, and 15%, were prepared to employ the sol-gel technique. Structural characterization of the synthesized materials was done by powder X-ray Diffraction and Raman studies. The optical UV-Visible spectroscopy provides the optical properties of $CoFe_2O_4$ and Nd-doped $CoFe_2O_4$ and the XPS spectra, which identify the constituting elements with their oxidation states, confirm the incorporation of Nd into the $CoFe_2O_4$ lattice. SEM was performed to investigate their surface morphology, showing the self-assembled microstructures of $CoFe_2O_4$. The dye degradation process was investigated for the synthesized samples with methylene blue dye using UV-Visible spectroscopy, which reveals the photocatalytic performance of pure $CoFe_2O_4$ and Nd doped $CoFe_2O_4$ by measuring the absorbance of methylene blue at the same interval of time. The 5% Nd doped $CoFe_2O_4$ exhibits enhanced photocatalytic activity with a degradation efficiency of 72% within 4 hours, which is higher than the pure sample.

Keywords: Neodymium doped $CoFe_2O_4$ nanoparticles; ferriets; optical properties; dye degradation; photocatalyst

1. Introduction

The demand for pure water for a sustainable life is increasing daily. On the other hand, releasing pollutants into the water system from various sources has become inevitable. In particular, the discharge of several dyes from textile industries contaminates water bodies[1–5]. Though the effluents in wastewater can be removed by physical methods like adsorption method, membrane filtration, ion exchange, and coagulation method, their usage is restricted as they are time-consuming methods, require special filtration techniques, and also do not degrade the dye to the fullest [6,7]. The biological treatments also failed to remove these carcinogenic dyes as they have more complex structures [8]. Hence, the researchers are looking for an environmentally friendly method to remove these dyes. This paves the way for developing a new method that uses solar energy as a light source to degrade toxic dyes, called the photocatalytic dye degradation process.

Semiconductor nanoparticles as photocatalysts are more cost-effective, technologically viable, and environmentally friendly materials [9]. The most commonly used photocatalysts, such as TiO_2, MoS_2, CdS, and SiO_2 are not adapted to the fullest as they have poor charge carrier separation, photo corrosion and stability, and a band gap in the UV region [10,11]. Thus, the improved chemical and physical durability and greater catalytic activity of metal oxides help overcome the challenges of applying pure metal nanoparticles. The nanomaterials with magnetic properties can be employed as catalysts under ambient conditions as these properties will help in improving their reutilization potential, thereby reducing the cost of the process [12.13]. Spinel ferrites that are nanosized have recently attracted attention in the field of materials science because of their numerous technological uses as well as their potential for understanding the principles of nanomagnetism [14,15]. Spinel ferrites have the formula $[MnFe_{1-n}][M_{1-n}Fe_{1+n}]O_4$ where n denotes the distribution of cations, M is a divalent metal cation [M = Cu^{2+}, Co^{2+}, Ni2+, and Sn^{2+}] and Fe is a trivalent metal cation [16-18]. Among many

ferrites, the cobalt ferrite has attracted more because of the combination of semiconducting and magnetic properties such as high coercivity [19], high positive anisotropy [20], high saturation magnetization [21], and chemical stability [22]. The $CoFe_2O_4$ is low bang gap semiconductor about 1.08ev and is highly stable to act as a photocatalyst [23]. As it has both photocatalytic and ferromagnetic properties, it can be used for oxidation and reduction reactions in UV and visible light [24]. Also, $CoFe_2O_4$ is significant in the thermal decomposition of O-O bonds and in the elimination of oxides [25]. Despite its advantages, the recombination rate of $CoFe_2O_4$ is the major issue in attaining its highest efficiency. However, this can be overcome by the doping of metal ions. In particular, adding rare earth elements to pure semiconductors improve photocatalytic efficiency by allowing functional groups to form complexes via interactions of f orbital rare earth metals [26]. The earlier investigations revealed that the doping of Nd^{3+} on TiO_2 increases the carrier lifetime facilitates charge movement, and functions as a direct trapping spot [27]. In addition, it is seen that rare earth doping such as Eu^{3+} and Nd^{3+} in semiconductor photocatalyst makes it activated in the visible region by increasing its optical adsorption and generating a high number of electron-hole pairs, thereby enhancing their photocatalytic performance [28]. Among many methods that have been employed to synthesize $CoFe_2O_4$, such as hydrothermal [29], microemulsion method [30], and co-precipitation [31], the gel matrix method was adopted to fabricate uniform self-assembly [32,33].

Herein, the preparation of pure and Nd-doped $CoFe_2O_4$ by the gel matrix technique was reported. XRD, Raman, and SEM were used to study the structure and morphology of the synthesized particles. The optical properties were examined by UV-Visible spectra, and the elemental identification with their oxidation state was done by XPS analysis. The photocatalytic activity of $CoFe_2O_4$ and Nd-doped $CoFe_2O_4$ was studied by performing a dye degradation process.

2. Experimental Methods

2.1 Materials

Ferric nitrate nanohydrate ($Fe(No_3)_3.9H_2O$, Loba), Cobalt (II) nitrate hexahydrate ($Co(No_3)_2.6H_2O$, Merck), Neodymium nitrate hexahydrate ($Nd(No_3)_3.6H_2O$), Citric acid monohydrate ($C_6H_8O_7.H_2O$, Sisco), Ethylene glycol ($C_2H_6O_2$, Hi Media) were used without being purified in any way.

2.2 Synthesis of $CoFe_2O_4$ and Nd doped $CoFe_2O_4$ nanoparticles

The gel matrix method was employed to synthesize the $CoFe_2O_4$ nanoparticles and Nd-doped $CoFe_2O_4$ nanoparticles with various concentrations of Neodymium nitrate. In particular, 1 milli mole of $Co(No_3)_2.6H_2O$ and 1 milli mole of $Fe(No_3)_3.9H_2O$ were dissolved in two separate beakers containing 25 mL of deionized water. These solutions were stirred thoroughly until they were completely dissolved in water. Then the above two solutions were mixed, adding 2 milli moles of citric acid monohydrate ($C_6H_8O_7.H_2O$), forming a citrate complex. After stirring for about 20 min, the inducing agent, ethylene glycol, was added to polymerize the separated citrate complex [34]. As prepared, gel flakes were heated at 250 °C, and samples were annealed at 650 °C for an hour. The same method was used to synthesize Neodymium doped $CoFe_2O_4$ with various percentages of neodymium concentration, such as 5, 10, and 15%. The 5% of $Nd(NOo)_3.6H_2O$ is added to $Co(NO_3)_2.6H_2O$ and dissolved in 25 mL of deionized water. This is followed by the mixing with $Fe(NO_3)_3.9H_2O$ that has been dissolved in 25 mL of dissolved water separately. Then the citric acid is added, and the above procedure is adopted, resulting in the formation of black-colored Nd doped $CoFe_2O_4$ nanoparticles. The 10 and 15 % of Nd doped CoFe2O4 nanoparticles were synthesized by performing the same.

2.3 Characterisation techniques

PANalytical X-ray Diffraction (XRD) with CuKα radiation of λ =1.5405 Å was used to investigate the crystallinity of synthesized $CoFe_2O_4$ nanoparticles and Nd doped $CoFe_2O_4$

nanoparticles. A Jobin Yuvon HR 800 Raman spectrometer with a 532nm laser source was used for Raman spectral analysis. The optical absorption of syntheised samples was studied with a Thermofisher UV–visible spectrophotometer. X-ray photoelectron spectroscopy (XPS), performed through Thermo Scientific K-Alpha Surface Analysis and was used to identify constituents of synthesized nanoparticles. Scanning Electron Microscopy (SEM) ZEISS EVO 18 was used to examine the changes in surface structure caused by the addition of dopants. The UV-Visible absorbance was measured using a Shimazu UV/Visible 1380 UV/Vis-NIR spectrophotometer to record methylene blue degradation.

2.4 Photocatalytic performance

Methylene blue dye degradation under white light (100 W mercury lamp) was used to assess the photocatalytic activity. In an aqueous solution of MB (50 mL), 50 mg of $CoFe_2O_4$ was completely dissolved. Dark stirring was performed to balance the absorption−desorption process of the as-prepared dye before light illumination. Under irradiation, the samples were collected at a regular time interval of one hour and centrifuged to remove the residue of particles from the solution. The efficiency of degradation of the photocatalyst was calculated as follows [35]:

$$\text{Degradation efficiency} = \frac{A_0 - A_t}{A_0} \times 100\%$$

where A_0 - absorbance at the time being zero and A_t - absorbance at a particular time. Due to the magnetic properties of pure and Nd-doped $CoFe_2O_4$, nano self-assembly may be readily removed from the treated solution using a magnetic separation approach, leaving no secondary pollution during the degradation process. As an outcome, $CoFe_2O_4$ and Nd-doped $CoFe_2O_4$ nanoparticles are beneficial materials in photocatalytic dye degradation. The kinetic behavior of degradation of methylene blue process is investigated using a pseudo-first-order equation [36], which is given as follows:

$$ln\left(\frac{C_0}{C}\right) = kt$$

Where C_0 - initial concentration of dye (mg L^{-1}), C - concentration of dye at a particular time t (mg L^{-1}), k - rate constant ($hour^{-1}$), and t - irradiated time (hour).

3. RESULT AND DISCUSSION

3.1 Structural studies

XRD patterns of synthesized $CoFe_2O_4$ and Nd-doped $CoFe_2O_4$ nanoparticles with 5, 10, and 15% of Nd are depicted in Figure 1. The observed pattern was well matched with standard $CoFe_2O_4$ (JCPDS card No.-010746403). The structure of $CoFe_2O_4$ seems to be cubic with a space group of Fd-3m. Lattice constants of $CoFe_2O_4$ were found to be a = b = c = 8.3860 [37]. The reflections at 2θ values of 30.1°, 35.4°, 43.1°, 57.0°, and 62.6° in the (220), (311), (400), (511), and (440) planes, respectively, indicates better growth of crystal structure. The doping of Nd into pure $CoFe_2O_4$, broadens the peaks of $CoFe_2O_4$, indicating that the crystallite size of $CoFe_2O_4$ is reduced. The broadening of peaks signifies the nanoscale features of $CoFe_2O_4$.

3.2 Raman Analysis

Figure 2 depicts the obtained Raman spectra of pure $CoFe_2O_4$ and Nd-doped $CoFe_2O_4$ with various percentages of Nd, such as 5, 10, and 15%. The inverse spinel structure of $CoFe_2O_4$ nanoparticles with cubic O_h^7 symmetry [38]. According to group theory, $A_{1g}+E_g+3T_{2g}$ are the five modes that are active Raman states for $CoFe_2O_4$ [39]. The vibrations of Fe^{3+} at the octahedral site correspond to a peak at 470 cm^{-1}, whereas the vibrations of Co^{2+} at the tetrahedral site correspond to a peak at 670 cm^{-1}. In a tetrahedral vacancy in FeO_4, the A_{1g} mode represents the symmetric stretching of an oxygen atom with respect to a metal ion. Eg and T2g modes are produced by the symmetric and anti-symmetric bending of the O atom in the Fe-O

or Co-O link at the octahedral and tetrahedral voids [40]. An additional peak at 620 cm^{-1} with A1g symmetry occurs because the octahedral and tetrahedral locations exchange cations [41]. Adding Nd to $CoFe_2O_4$ results in red shifting; the peak at 690 cm^{-1} shifted towards a lower wavenumber. Similar wavenumber shifting patterns have previously been reported for rare earth element doping [42]. Also, the doping of Nd to pure $CoFe_2O_4$ causes a redistribution of Fe^{3+} ions and Co^{2+} ions. Thus, Fe^{3+} moves to tetrahedral sites, and Co^{2+} moves to octahedral sites, resulting in an increased inversion degree of spinel ferrites.

3.3 Optical properties

Absorption characteristics of $CoFe_2O_4$ and Nd-doped $CoFe_2O_4$ were examined using UV-visible spectroscopy. Figures 3a and 3b show the UV-visible absorption and reflectance spectra of synthesized pure and Nd doped $CoFe_2O_4$ recorded in the 200-400 nm range, respectively. The Fe -O charge transfer of an isolated Fe^{3+} ion in octahedral coordination is responsible for the band at 232 nm [43]. Comparing $CoFe_2O_4$ nanoparticles to 5% Nd doped $CoFe_2O_4$, it is clear that the absorption edge gradually moves toward the higher wavelength. This is due to intrinsic bandgap absorption. An electronic transfer between the valence and conduction bands causes these peaks. The exchange interaction between the s-f and d-f orbits causes a negative and positive adjustment to the edges of the conduction and valence bands, resulting in a reduction in the band gap.

3.4 XPS

Chemical stoichiometry of as-synthesized pure and Nd-doped $CoFe_2O_4$ was determined using XPS. Recorded XPS spectra corresponding to Co 2p, Fe 2p, O 1s, and Nd 3d core levels of synthesized samples are presented in Figure 4. The peaks that emerged at 779 and 794 eV correspond to Co $2p_{3/2}$ and $2p_{1/2}$, respectively, confirming the presence of Co^{2+} state [44], as shown in Figure 4a. Figure 4b gives the Fe 2p spectra, and the peak positions around 708 and

723 eV correspond to Fe $2p_{3/2}$ and Fe $2p_{1/2}$ for Fe^{3+} states, revealing the oxidation state of iron is Fe^{3+} and not Fe^{2+} [45]. Binding energy obtained at 531.7 eV for oxygen species (O 1s) agrees with the standard and is presented in Figure 4c [46]. XPS spectrum of Nd 3d is shown in Figure 4d. It is observed that doping of Nd to $CoFe_2O_4$ results in the shifting of peaks to higher values in Co 2p, Fe 2p, and O 1s spectra. The Nd 3d core level photoemission peaks at 982 and 1004 eV correlate to the 5/2 and 3/2 spin-orbit double components, respectively, showing that Nd ions exist in a trivalent state. Thus, the XPS results confirm the successful incorporation of Nd atoms into the $CoFe_2O_4$ lattice [47].

3.5 Surface Morphology

The SEM image of as-synthesized pure $CoFe_2O_4$ and Nd doped with various concentrations of Nd, such as 5, 10, and 15%, is shown in Figure 5. The $CoFe_2O_4$ shows the self-assembled microstructure. The synthesized nanoparticles appeared to be brick in which the top and bottom surfaces were flat while the porous were developed along their sides. The particles seemed to be large and irregular agglomerates with veins in them. Large cracks appeared along its side, with porosity here and there. The veins are arranged in a random manner with some cuts in them. In some regions of the surface, wrinkles and some porous cracks appear. Adding dopant to pure $CoFe_2O_4$ seems to increase the porous formation and develop patches on the top and bottom of the surface. Also, the doping of Nd results in the formation of macroporous parallel to each other in which the microporous are grown inside the wall of them. Also, the wrinkles on the surface seemed to be enlarged after doping Nd. Increasing the amount of Nd doping increases the wrinkles throughout the surface. The patches developed on the wrinkled surface exhibit a porous structure. Further magnification reveals the presence of a vein-like structure inside the porous.

3.4 Photocatalytic performance

To investigate the photocatalytic performance of $CoFe_2O_4$ and Nd-doped $CoFe_2O_4$, Methylene Blue dye was degraded with the synthesized photocatalyst. Figure 6 depicts the absorbance of MB dye in the presence of $CoFe_2O_4$ and various percentages of Nd-doped $CoFe_2O_4$ photocatalysts. The decrease in absorbance at 664 nm, the characteristic absorbance peak of methylene blue dye, specifies that the MB dye degrades faster in the presence of a catalyst. Under light irradiation, the electrons get shifted from the valence band to the conduction band, leaving their associated holes in the valence band. These valence band holes produce $^{\cdot}OH$ radical by reacting with OH^-, which is present in the water. The photoinduced electrons are captured by O_2, resulting in the formation of superoxide anion $^{\cdot}O_2^-$. The generated $^{\cdot}OH$ and $^{\cdot}O_2^-$ is responsible for the oxidation process in the degradation of methylene blue dye. The shifted electrons shortly recombine with the holes in the valence band in $CoFe_2O_4$. To reduce such faster recombination, doping of rare earth metal ions, particularly Nd^{3+}, was done. The doping of Nd^{3+} significantly alters the band structure of $CoFe_2O_4$ as it forms the localized energy level in $CoFe_2O_4$. The reaction mechanism of $CoFe_2O_4$ and Nd-doped $CoFe_2O_4$ as photocatalysts is as follows:

$$CoFe_2O_4 + h\upsilon \rightarrow CoFe_2O_4\ (e^- + h^+) \quad (3)$$

$$H_2O + CoFe_2O_4\ (h^+) \rightarrow CoFe_2O_4 + {}^{\cdot}OH + H^+ \quad (4)$$

$$Nd^{3+} + O_2 \rightarrow Nd^{4+} + {}^{\cdot}O_2^- \quad (5)$$

$$CoFe_2O_4\ (e^-) + Nd^{4+} \rightarrow CoFe_2O_4 + Nd^{3+} \quad (6)$$

$${}^{\cdot}O_2^- + H^+ \rightarrow {}^{\cdot}HO_2 \quad (7)$$

$${}^{\cdot}HO_2 + {}^{\cdot}HO_2 \rightarrow H_2O_2 + O_2 \quad (8)$$

$$H_2O_2 + {}^{\cdot}O_2^- \rightarrow {}^{\cdot}OH + OH^- + O_2 \quad (9)$$

$$MB + {}^{\cdot}OH/{}^{\cdot}O_2^-/H_2O_2 \rightarrow \text{degraded products} \quad (10)$$

The degrading efficiency of $CoFe_2O_4$ and various percentages of Nd-doped $CoFe_2O_4$ photocatalysts is evaluated using equation (1) [48], as shown in Figure 7. It is seen that $CoFe_2O_4$ degrades MB solution by about 67% within 4 hours. To enhance the degrading efficiency of $CoFe_2O_4$, the doping of various percentage rare earth metal ions was carried out. Within the same time period, the degradation efficiency of 5% Nd doped $CoFe_2O_4$ is 72% higher than that of $CoFe_2O_4$. On the other hand, the increase in the percentage of Nd doping in $CoFe_2O_4$ decreases the degradation efficiency, such as 69% and 61% for 10% and 15% Nd doped $CoFe_2O_4$, respectively, for a reaction time of 4 hours. This reveals that raising the concentration of Nd doping favors the interaction between Nd trivalent metal ions ($Nd^{3+)}$ and $CoFe_2O_4$, resulting in the shattering of the $CoFe_2O_4$ sites. This site splitting results in less electron-hole separation and a slower oxidation process, thereby diminishing the photocatalytic performance. Thus, the dye degradation efficiency appears to be enhanced only by doping low concentrations of Nd^{3+}. The comparison of the photocatalytic activity of $CoFe_2O_4$ and various percentages of Nd-doped $CoFe_2O_4$ with previous works is tabulated in table 1.

Figure 8 shows the kinetic behavior of the deterioration process of MB dye with the synthesized photocatalyst. A straight line was obtained. The R^2 value and the rate of degradation constant were tabulated in table 2. The 5% Nd-doped $CoFe_2O_4$ degrades the dye at a higher rate of 0.3243 $hour^{-1}$. Thus, the doping of Nd to $CoFe_2O_4$ boosts the MB dye degradation process, which agrees with the resultant efficiency. Due to their ease of separation and lack of secondary contamination during the reaction, the synthesized nanoparticles, such as $CoFe_2O_4$ and Nd-doped $CoFe_2O_4$ may be used in several repeating processes.

4. Conclusion

The $CoFe_2O_4$ and Nd doped $CoFe_2O_4$ with various percentages of doping, such as 5, 10, and 15%, were effectively synthesized using the sol-gel process. XRD studies confirm the

cubic structure of $CoFe_2O_4$. The Raman investigation was used to determine the photocatalyst's numerous vibrational modes and phase impurities. XPS spectra confirmed the Nd incorporation in the $CoFe_2O_4$ lattice as Nd^{3+}. SEM images depict flat surfaces of $CoFe_2O_4$ on top and bottom, with porous structures forming along its sides. Degradation of Methylene Blue dye with synthesized photocatalysts such as $CoFe_2O_4$ and Nd-doped $CoFe_2O_4$ revealed that doping Nd to $CoFe_2O_4$ increases photocatalytic activity. The 5% Nd doped $CoFe_2O_4$ shows higher photocatalytic performance, with a degradation efficiency of about 72% within 4 hours.

Conflict of interests statement

There is no conflict of interests from authors of this manuscript.

Data availability statement

The raw/processed data required to reproduce these findings cannot be shared at this time as the data also forms part of an ongoing study.

Acknowledgement

The authors extend their appreciation to the Research Center for Advanced Materials Science (RCAMS), King Khalid University, Saudi Arabia, for funding this work under grant number RCAMS/KKU/020-22.

Credit Author Statement

S. Hemasankari, S. Priyadharshini, D. Thangaraju, V. Sathiyanarayanamoorthi , Njod Mansour Hasan Alsdran, Mohd. Shkir: Conceptualization, Methodology, Investigation, Writing – Original Draft, Writing – Review & Editing.**:** Writing – Review & Editing, Review and Validation and Funding acquisition.

References

[1] A. Rafiq, M. Ikram, S. Ali, F. Niaz, M. Khan, Q. Khan, M. Maqbool, Photocatalytic degradation of dyes using semiconductor photocatalysts to clean industrial water pollution, J. Ind. Eng. Chem. 97 (2021) 111–128.

[2] A.S. Kshirsagar, P.K. Khanna, Titanium dioxide (TiO_2)-decorated silver indium

diselenide (AgInSe2): Novel nano-photocatalyst for oxidative dye degradation, Inorg. Chem. Front. 5 (2018) 2242–2256.

[3] D.C. and Y.C. and N.Z. and P.C. and Y.W. and K.L. and S.H. and P.C. and P.P. and R.Z. and L.W. and H.L. and Y.L. and R. Ruan, Photocatalytic degradation of organic pollutants using TiO_2-based photocatalysts: a review, J. Clean. Prod. 268 (2020) 121725.

[4] A.P. Naik, A. V. Salkar, M.S. Majik, P.P. Morajkar, Enhanced photocatalytic degradation of Amaranth dye on mesoporous anatase TiO_2: Evidence of C-N, NN bond cleavage and identification of new intermediates, Photochem. Photobiol. Sci. 16 (2017) 1126–1138.

[5] M. Aqeel, M. Rashid, M. Ikram, A. Haider, S. Naz, J. Haider, A. Ul-Hamid, A. Shahzadi, Photocatalytic, dye degradation, and bactericidal behavior of Cu-doped ZnO nanorods and their molecular docking analysis, Dalt. Trans. 49 (2020) 8314–8330.

[6] T. Thilagavathi, D. Venugopal, R. Marnadu, J. Chandrasekaran, D. Thangaraju, B. Palanivel, M.S. Hamdy, M. Shkir, H.E. Ali, $WO_3/CoWO_4$ nanocomposite synthesis using a facile co-precipitation method for enhanced photocatalytic applications, J. Phys. Chem. Solids. 154 (2021) 110066.

[7] Y.M. Hunge, A.A. Yadav, V.L. Mathe, Ultrasound assisted synthesis of WO_3-ZnO nanocomposites for brilliant blue dye degradation, Ultrason. Sonochem. 45 (2018) 116–122.

[8] S. Guo, G. Zhang, J. Wang, Photo-Fenton degradation of rhodamine B using Fe_2O_3-Kaolin as heterogeneous catalyst: Characterization, process optimization and mechanism, J. Colloid Interface Sci. 433 (2014) 1–8.

[9] Q. Sun, K. Li, S. Wu, B. Han, L. Sui, L. Dong, Remarkable improvement of TiO_2 for dye photocatalytic degradation by a facile post-treatment, New J. Chem. 44 (2020) 1942–1952.

[10] G.S. Selvam, T. Dheivasigamani, A. Prabhu, N.K. Mani, Embellishing 2-D MoS_2 Nanosheets on Lotus Thread Devices for Enhanced Hydrophobicity and Antimicrobial Activity, ACS Omega. 7 (2022) 24606–24613.

[11] E. Pakdel, W.A. Daoud, S. Seyedin, J. Wang, J.M. Razal, L. Sun, X. Wang, Tunable photocatalytic selectivity of TiO_2/SiO_2 nanocomposites: Effect of silica and isolation approach, Colloids Surfaces A Physicochem. Eng. Asp. 552 (2018) 130–141.

[12] C. Singh, A. Goyal, S. Singhal, Nickel-doped cobalt ferrite nanoparticles: Efficient catalysts for the reduction of nitroaromatic compounds and photo-oxidative degradation of toxic dyes, Nanoscale. 6 (2014) 7959–7970.

[13] M. Kundu, B. Mondal, D. Das, U.K. Roy, Synthesis and Reactivity of Copper and Copper Containing Magnetically Separable Catalysts, ChemistrySelect. 7 (2022) e202104543.

[14] B. Mondal, M. Kundu, S.P. Mandal, R. Saha, U.K. Roy, A. Roychowdhury, D. Das, Sonochemically Synthesized Spin-Canted $CuFe_2O_4$ Nanoparticles for Heterogeneous Green Catalytic Click Chemistry, ACS Omega. 4 (2019) 13845–13852.

[15] B.J. Sarkar, M. Kundu, B. Mondal, S. Mukherjee, A. Bandyopadhyay, U.K. Roy, Microstructural investigation of sonochemically synthesized Zn substituted $CuFe_2O_4$ nanoparticles for heterogeneous green catalytic click chemistry and dye degradation, J. Mol. Struct. 1274 (2023) 134493.

[16] S.M. Nikam, A. Sharma, M. Rahaman, A.M. Teli, S.H. Mujawar, D.R.T. Zahn, P.S.

Patil, S.C. Sahoo, G. Salvan, P.B. Patil, Pulsed laser deposited $CoFe_2O_4$ thin films as supercapacitor electrodes, RSC Adv. 10 (2020) 19353–19359.

[17] C. Himcinschi, I. Vrejoiu, G. Salvan, M. Fronk, A. Talkenberger, D.R.T. Zahn, D. Rafaja, J. Kortus, Optical and magneto-optical study of nickel and cobalt ferrite epitaxial thin films and submicron structures, J. Appl. Phys. 113 (2013).

[18] X. Zeng, J. Zhang, S. Zhu, X. Deng, H. Ma, J. Zhang, Q. Zhang, P. Li, D. Xue, N.J. Mellors, X. Zhang, Y. Peng, Direct observation of cation distributions of ideal inverse spinel $CoFe_2O_4$ nanofibres and correlated magnetic properties, Nanoscale. 9 (2017) 7493–7500.

[19] A.S. Ponce, E.F. Chagas, R.J. Prado, C.H.M. Fernandes, A.J. Terezo, E. Baggio-Saitovitch, High coercivity induced by mechanical milling in cobalt ferrite powders, J. Magn. Magn. Mater. 344 (2013) 182–187.

[20] N.V. Long, Y. Yang, T. Teranishi, C.M. Thi, Y. Cao, M. Nogami, Related magnetic properties of $CoFe_2O_4$ cobalt ferrite particles synthesised by the polyol method with $NaBH_4$ and heat treatment: new micro and nanoscale structures, RSC Adv. 5 (2015) 56560–56569.

[21] S.K. Gore, R.S. Mane, M. Naushad, S.S. Jadhav, M.K. Zate, Z.A. Alothman, B.K.N. Hui, Influence of Bi^{3+}-doping on the magnetic and Mössbauer properties of spinel cobalt ferrite, Dalt. Trans. 44 (2015) 6384–6390.

[22] D. Zhao, X. Wu, H. Guan, E. Han, Study on supercritical hydrothermal synthesis of $CoFe_2O_4$ nanoparticles, J. Supercrit. Fluids. 42 (2007) 226–233.

[23] A. Kalam, A.G. Al-Sehemi, M. Assiri, G. Du, T. Ahmad, I. Ahmad, M. Pannipara, Modified solvothermal synthesis of cobalt ferrite ($CoFe_2O_4$) magnetic nanoparticles

photocatalysts for degradation of methylene blue with H_2O_2/visible light, Results Phys. 8 (2018) 1046–1053.

[24] L. Gan, S. Shang, C.W.M. Yuen, S.X. Jiang, E. Hu, Hydrothermal synthesis of magnetic $CoFe_2O_4$ /graphene nanocomposites with improved photocatalytic activity, Appl. Surf. Sci. 351 (2015) 140–147.

[25] S. Huang, Y. Xu, M. Xie, Y. Ma, J. Yan, Y. Li, Y. Zhao, H. Xu, H. Li, Multifunctional C-Doped $CoFe_2O_4$ Material as Cocatalyst to Promote Reactive Oxygen Species Generation over Magnetic Recyclable C-CoFe/Ag-AgX Photocatalysts, ACS Sustain. Chem. Eng. 6 (2018) 11968–11978.

[26] U. Alam, A. Khan, D. Ali, D. Bahnemann, M. Muneer, Comparative photocatalytic activity of sol-gel derived rare earth metal (La, Nd, Sm and Dy)-doped ZnO photocatalysts for degradation of dyes, RSC Adv. 8 (2018) 17582–17594.

[27] B. Trujillo-Navarrete, M. del Pilar Haro-Vázquez, R.M. Félix-Navarro, F. Paraguay-Delgado, H. Alvarez-Huerta, S. Pérez-Sicairos, E.A. Reynoso-Soto, Effect of Nd^{3+} doping on structure, microstructure, lattice distortion and electronic properties of TiO_2 nanoparticles, J. Rare Earths. 35 (2017) 259–270.

[28] D.M. Tobaldi, R.A.S. Ferreira, R.C. Pullar, M.P. Seabra, L.D. Carlos, J.A. Labrincha, Nano-titania doped with europium and neodymium showing simultaneous photoluminescent and photocatalytic behaviour, J. Mater. Chem. C. 3 (2015) 4970–4986.

[29] V. Georgiadou, V. Tangoulis, I. Arvanitidis, O. Kalogirou, C. Dendrinou-Samara, Unveiling the physicochemical features of $CoFe_2O_4$ nanoparticles synthesized via a variant hydrothermal method: NMR relaxometric properties, J. Phys. Chem. C. 119 (2015) 8336–8348.

[30] P. Laokul, S. Arthan, S. Maensiri, E. Swatsitang, Magnetic and Optical Properties of $CoFe_2O_4$ Nanoparticles Synthesized by Reverse Micelle Microemulsion Method, J. Supercond. Nov. Magn. 28 (2015) 2483–2489.

[31] M. Basak, M.L. Rahman, M.F. Ahmed, B. Biswas, N. Sharmin, Calcination effect on structural, morphological and magnetic properties of nano-sized $CoFe_2O_4$ developed by a simple co-precipitation technique, Mater. Chem. Phys. 264 (2021) 124442.

[32] B. Shunmughananthan, T. Dheivasigamani, J. Sthevan Kovil Pitchai, S. Periyasamy, Performance comparison of distinct bismuth molybdate single phases for asymmetric supercapacitor applications, Dalt. Trans. 51 (2022) 15579–15592.

[33] D. Thangaraju, A. Durairajan, D. Balaji, S. Moorthy Babu, Synthesis and characterization of monoclinic $KGd(WO_4)_2$ particles for non-cubic transparent ceramics, Opt. Mater. (Amst). 35 (2013) 753–756.

[34] J. Sthevan Kovil Pitchai, T. Dheivasigamani, B. Shunmughananthan, R. Arunagiri, S. Periyasamy, Single-wall and graphene-modified multiwall wasp nest shaped $Bi_2Mo_2O_9$ self-assembly for performance-enhanced asymmetric supercapacitor , J. Mater. Chem. C. 10 (2022) 16453–16464.

[35] T. Thiyagarajan, V. Deivasigamani, M. Raj, C. Joseph, T. Dheivasigamani, B. Palanivel, M.S. Hamdy, M. Shkir, Facile synthesis and characterization of $WO_3/CuWO_4$ nanocomposites for the removal of toxic methylene blue dye, Korean J. Chem. Eng. 38 (2021) 952–965.

[36] P. Shanmugam, T. Dheivasigamani, S. Moorthy Babu, M. Shkir, E. El Sayed Massoud, R. Marnadu, V.R. Minnam Reddy, A facile sol–gel synthesis and characterization of europium (Eu) doped β-$Bi_2Mo_2O_9$ nanoparticles with remarkably enhanced photocatalytic activity for waste-water treatments, Inorg. Chem. Commun.

146 (2022) 110163.

[37] B.J. Rani, M. Ravina, B. Saravanakumar, G. Ravi, V. Ganesh, S. Ravichandran, R. Yuvakkumar, Ferrimagnetism in cobalt ferrite ($CoFe_2O_4$) nanoparticles, Nano-Structures and Nano-Objects. 14 (2018) 84–91.

[38] K. Gandha, K. Elkins, N. Poudyal, J. Ping Liu, Synthesis and characterization of $CoFe_2O_4$ nanoparticles with high coercivity, J. Appl. Phys. 117 (2015).

[39] N. Liu, P. Du, P. Zhou, R.G. Tanguturi, Y. Qi, T. Zhang, C. Zhuang, Annealing temperature effects on the cation distribution in $CoFe_2O_4$ nanofibers, Appl. Surf. Sci. 532 (2020) 3–7.

[40] A. V. Ravindra, P. Padhan, W. Prellier, Electronic structure and optical band gap of $CoFe_2O_4$ thin films, Appl. Phys. Lett. 101 (2012) 1–5.

[41] T. Wang, T. Zhu, M. Brunet, C. Deshayes, P. Sciau, Raman study of Yuan Qinghua porcelain: the highlighting of dendritic $CoFe_2O_4$ crystals in blue decorations, J. Raman Spectrosc. 48 (2017) 267–270.

[42] F.R. Mariosi, J. Venturini, A. da Cas Viegas, C.P. Bergmann, Lanthanum-doped spinel cobalt ferrite ($CoFe_2O_4$) nanoparticles for environmental applications, Ceram. Int. 46 (2020) 2772–2779.

[43] M. Sundararajan, V. Sailaja, L. John Kennedy, J. Judith Vijaya, Photocatalytic degradation of rhodamine B under visible light using nanostructured zinc doped cobalt ferrite: Kinetics and mechanism, Ceram. Int. 43 (2017) 540–548.

[44] S. Ikram, J. Jacob, K. Mahmood, K. Mehboob, M. Maheen, A. Ali, N. Amin, S. Hussain, F. Ashraf, S.Z. Ilyas, A Kinetic study of Tb^{3+} and Dy^{3+} co-substituted $CoFe_2O_4$ spinel ferrites using temperature dependent XRD, XPS and SQUID

measurements, Ceram. Int. 46 (2020) 15943–15948.

[45] R.S. Gaikwad, S.-Y. Chae, R.S. Mane, S.-H. Han, O.-S. Joo, Cobalt Ferrite Nanocrystallites for Sustainable Hydrogen Production Application, Int. J. Electrochem. 2011 (2011) 1–6.

[46] S.R. Naik, A. V. Salker, Change in the magnetostructural properties of rare earth doped cobalt ferrites relative to the magnetic anisotropy, J. Mater. Chem. 22 (2012) 2740–2750.

[47] G. Vijayaprasath, R. Murugan, S. Palanisamy, N.M. Prabhu, T. Mahalingam, Y. Hayakawa, G. Ravi, Structural, optical and antibacterial activity studies of neodymium doped ZnO nanoparticles, J. Mater. Sci. Mater. Electron. 26 (2015) 7564–7576.

[48] V. Santhana, D. Thangaraju, A. Tanaka, W. Inami, S. JayaKumar, S. Matsuda, Development of Hybrid TiO_2/Paint Sludge Extracted Microbe Composite for Enhanced Photocatalytic Dye Degradation, J. Inorg. Organomet. Polym. Mater. 30 (2020) 2805–2813.

[49] C.M. Magdalane, G.M.A. Priyadharsini, K. Kaviyarasu, A.I. Jothi, G.G. Simiyon, Synthesis and characterization of TiO_2 doped cobalt ferrite nanoparticles via microwave method: Investigation of photocatalytic performance of congo red degradation dye, Surfaces and Interfaces. 25 (2021) 101296.

[50] J. Revathi, M.J. Abel, V. Archana, T. Sumithra, R. Thiruneelakandan, J. Joseph prince, Synthesis and characterization of $CoFe_2O_4$ and Ni-doped $CoFe_2O_4$ nanoparticles by chemical Co-precipitation technique for photo-degradation of organic dyestuffs under direct sunlight, Phys. B Condens. Matter. 587 (2020) 412136.

[51] S. Chen, D. Jiang, G. Zeng, H. Chi, L. Li, Y. He, F. Ke, J.D. Xiao, S. Ye, Dysprosium

doped $CoFe_2O_4$ with enhanced magnetic property and photodegradation activity of methyl orange, Mater. Lett. 284 (2021) 2–5.

[52] V. Mahdikhah, S. Saadatkia, S. Sheibani, A. Ataie, Outstanding photocatalytic activity of $CoFe_2O_4$ /rGO nanocomposite in degradation of organic dyes, Opt. Mater. (Amst). 108 (2020) 110193.

[53] N. Tariq, R. Fatima, S. Zulfiqar, A. Rahman, M.F. Warsi, I. Shakir, Synthesis and characterization of $MoO_3/CoFe_2O_4$ nanocomposite for photocatalytic applications, Ceram. Int. 46 (2020) 21596–21603.

[54] M. Sun, X. Han, S. Chen, Synthesis and photocatalytic activity of nano-cobalt ferrite catalyst for the photo-degradation various dyes under simulated sunlight irradiation, Mater. Sci. Semicond. Process. 91 (2019) 367–376.

[55] J. Parhizkar, M.H. Habibi, S.Y. Mosavian, Synthesis and Characterization of Nano $CoFe_2O_4$ Prepared by Sol-Gel Auto-Combustion with Ultrasonic Irradiation and Evaluation of Photocatalytic Removal and Degradation Kinetic of Reactive Red 195, Silicon. 11 (2019) 1119–1129.

[56] N. Abbas, N. Rubab, N. Sadiq, S. Manzoor, M.I. Khan, J.F. Garcia, I.B. Aragao, M. Tariq, Z. Akhtar, G. Yasmin, Aluminum-Doped Cobalt Ferrite as an Efficient Photocatalyst for the Abatement of Methylene Blue, Water. 12 (2020) 2285.

[57] D. Uzunoğlu, M. Ergüt, P. Karacabey, A. Özer, Synthesis of cobalt ferrite nanoparticles via chemical precipitation as an effective photocatalyst for photo fenton-like degradation of methylene blue, Desalin. Water Treat. 172 (2019) 96–105.

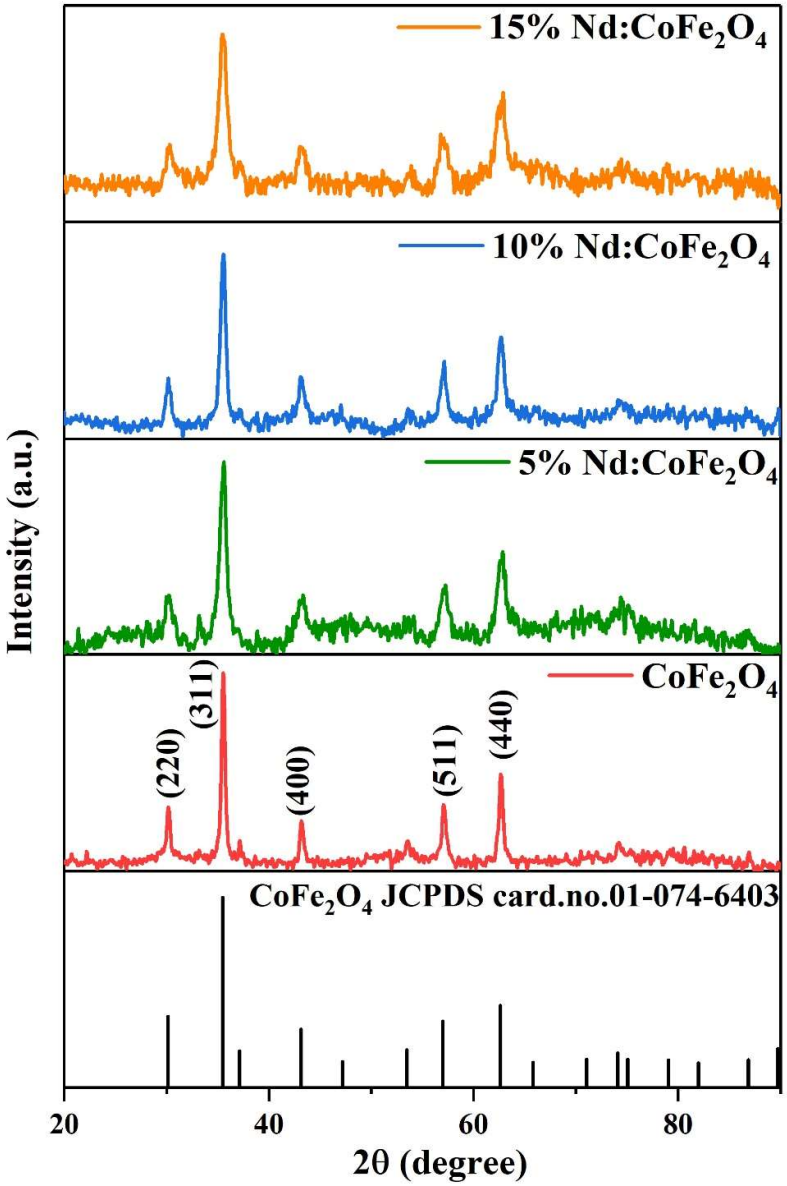

Figure 1: Comparitive XRD pattern of $CoFe_2O_4$, 5% Nd: $CoFe_2O_4$, 10% Nd: $CoFe_2O_4$ and 15% Nd: $CoFe_2O_4$.

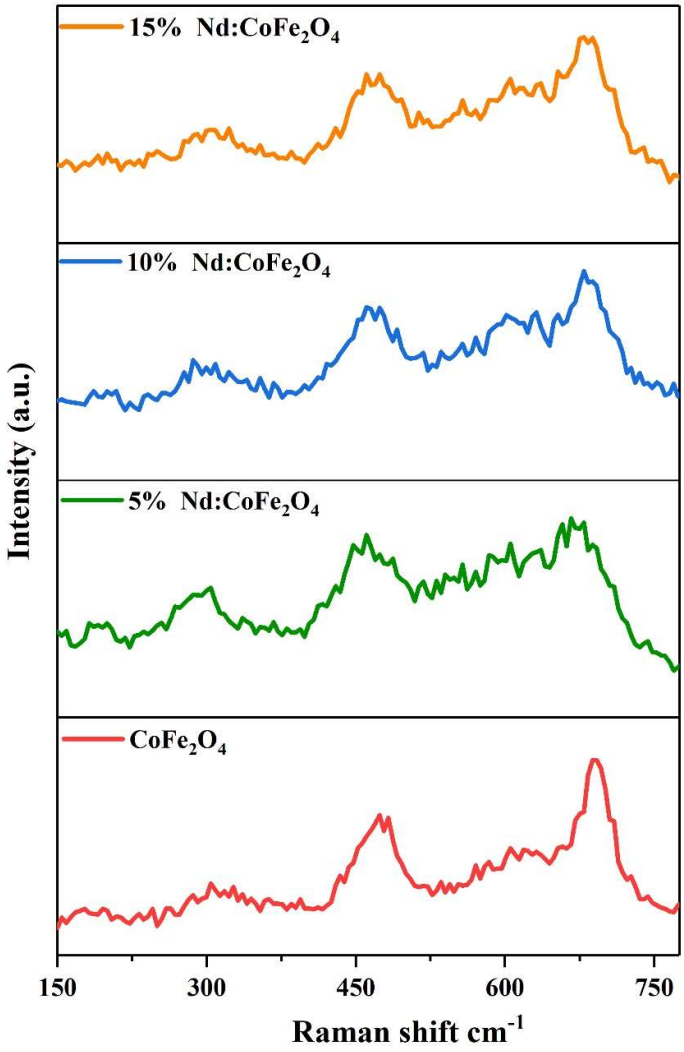

Figure 2: Comparative Raman spectra of $CoFe_2O_4$, 5% Nd: $CoFe_2O_4$, 10% Nd: $CoFe_2O_4$ and 15% Nd: $CoFe_2O_4$.

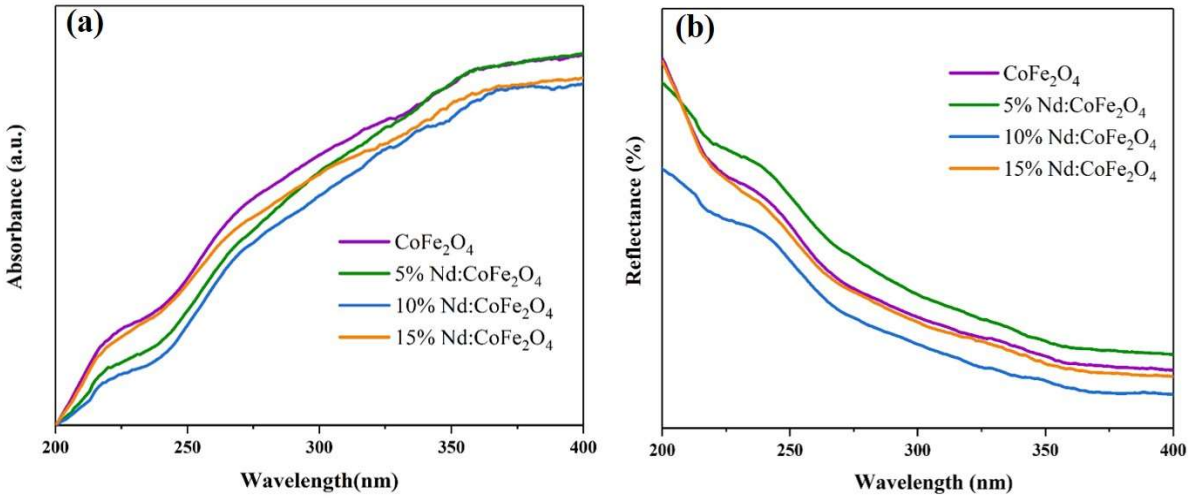

Figure 3: UV absorbance (a) and reflectance (b) spectra of $CoFe_2O_4$, 5% Nd: $CoFe_2O_4$, 10% Nd: $CoFe_2O_4$ and 15% Nd: $CoFe_2O_4$.

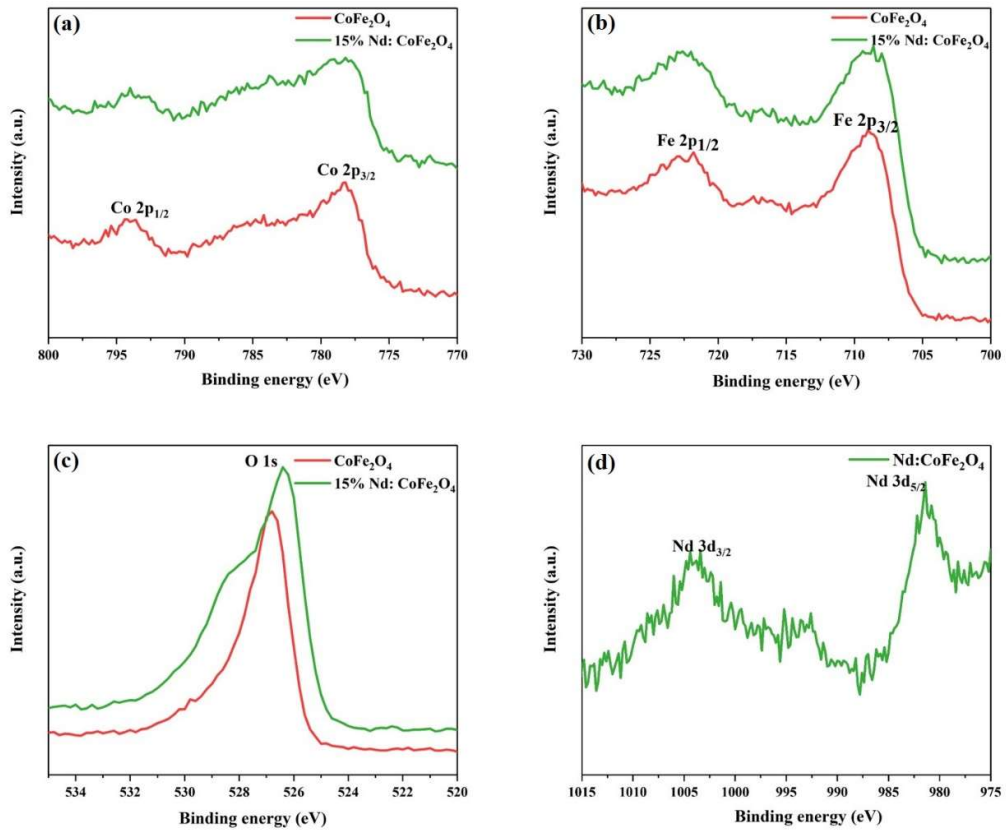

Figure 4: XPS graphs of Co 2p (a), Fe 2p (b), O 1s (c) and Nd 3d (d) for $CoFe_2O_4$ and 15% Nd: $CoFe_2O_4$

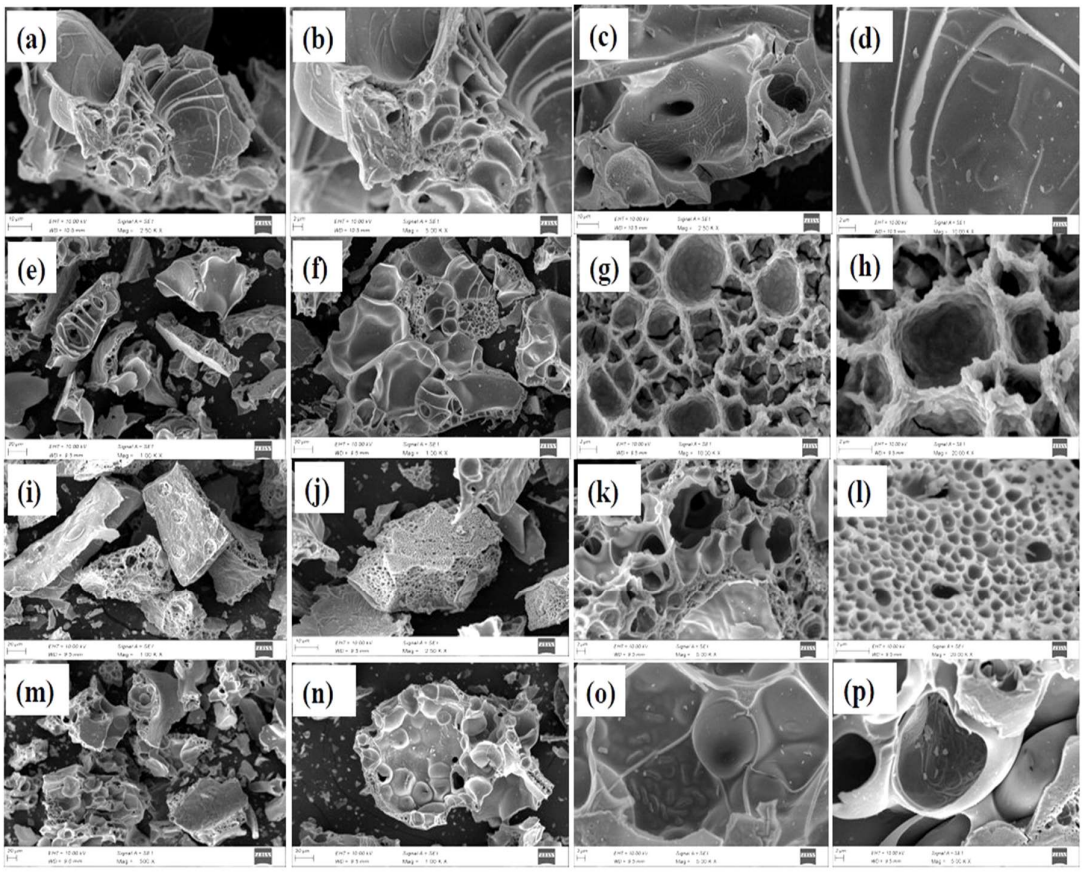

Figure 5: SEM images of $CoFe_2O_4$ (a-d), 5% Nd: $CoFe_2O_4$ (e-h), 10% Nd: $CoFe_2O_4$ (i-l) and 15% Nd: $CoFe_2O_4$ (m-p).

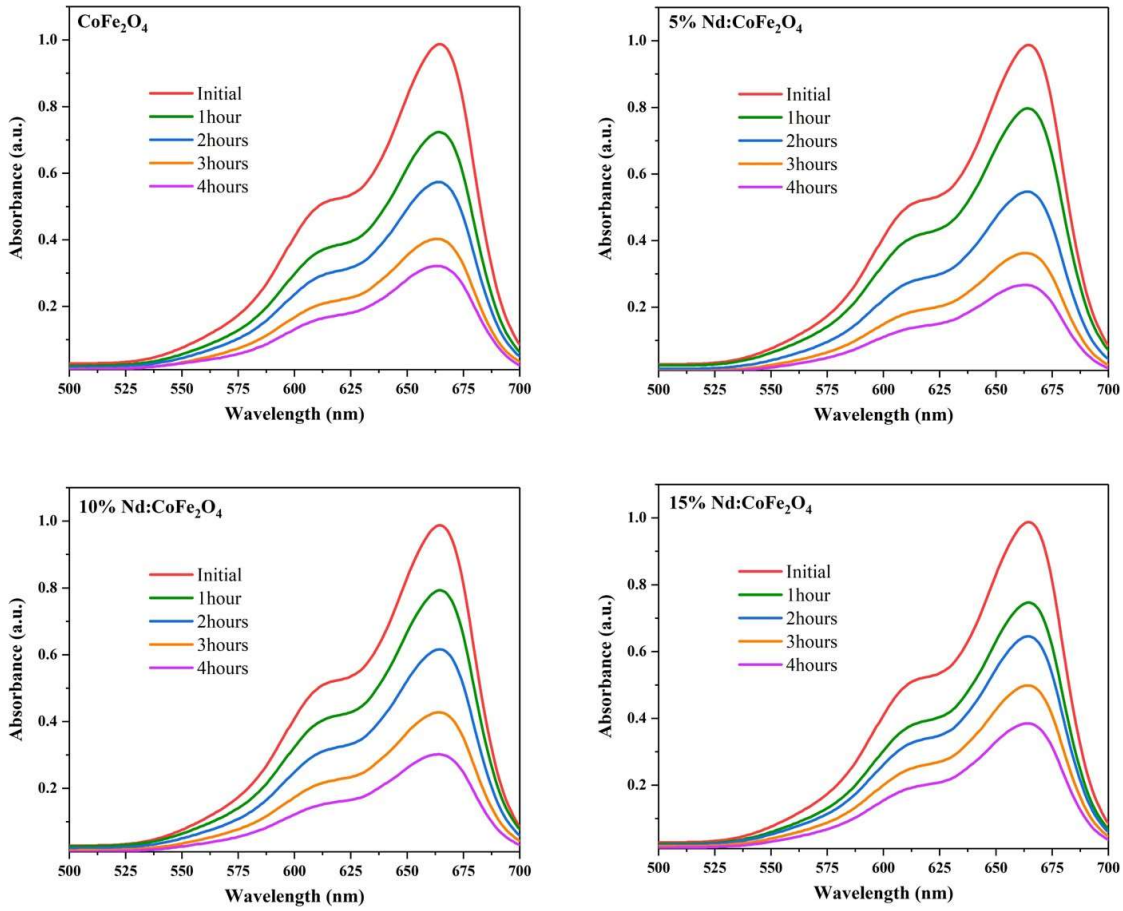

Figure 6: Photocatalytic degradation of methylene blue using $CoFe_2O_4$, 5% Nd: $CoFe_2O_4$, 10% Nd: $CoFe_2O_4$ and 15% Nd: $CoFe_2O_4$.

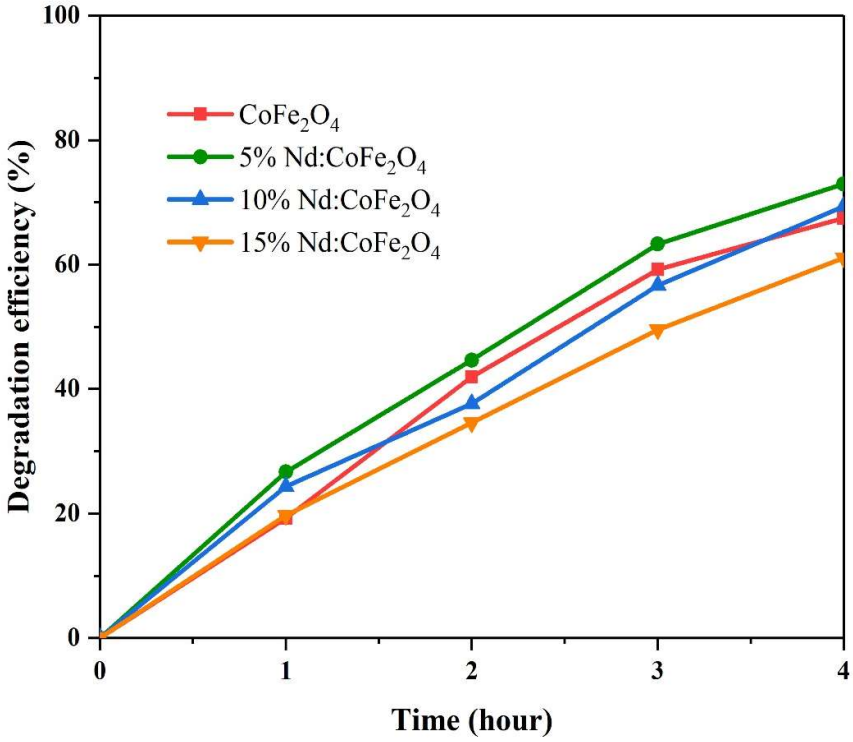

Figure 7: Degradation percentage of Methylene blue on $CoFe_2O_4$, 5% Nd: $CoFe_2O_4$, 10% Nd: $CoFe_2O_4$ and 15% Nd: $CoFe_2O_4$.

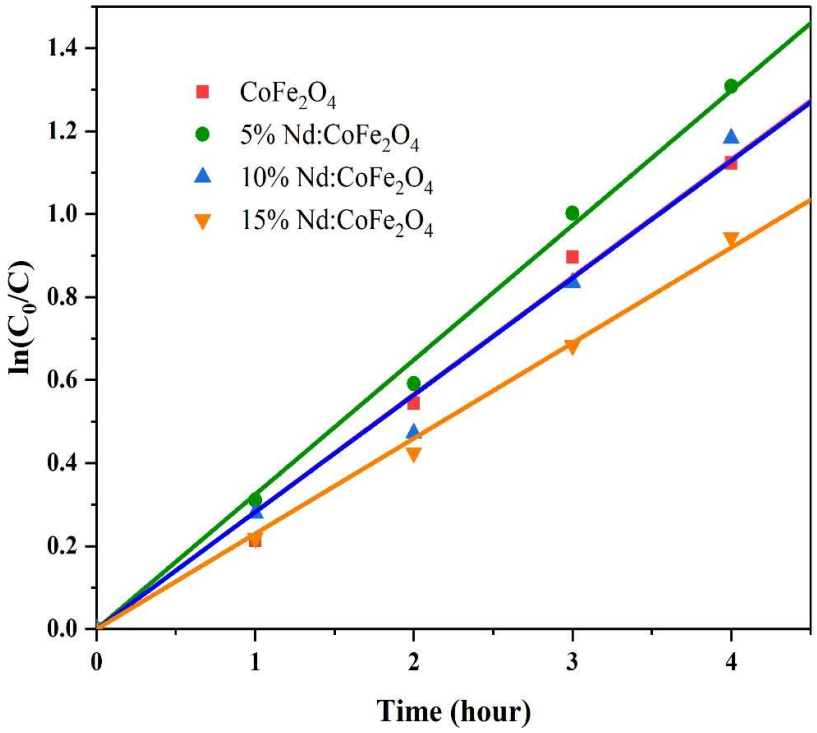

Figure 8: The kinetic plot for the degradation of methylene blue with $CoFe_2O_4$, 5% Nd: $CoFe_2O_4$, 10% Nd: $CoFe_2O_4$ and 15% Nd: $CoFe_2O_4$.

Table1: Photocatalytic activity of Nd doped $CoFe_2O_4$ in comparison to other previous reports.

Photocatalyst	Synthesis route	Model pollutant	Result	Ref
TiO2 doped $CoFe_2O_4$	Microwave method	Congo red	The photocatalytic activity was about 85 and 97% for catalyst and catalyst/H_2O_2 within 120 min of time.	[49]
Ni doped $CoFe_2O_4$	Co-precipitation	Methylene blue, Rhodamine B, Crystal violet	Degradation of MB, RhB and Crystal violet with Ni- $CoFe_2O_4$ was found to be 83.4, 63.62 and 82.76% respectively within 90 min of irradiation	[50]
Dy doped $CoFe_2O_4$	Co-precipitation	Methyl orange	The 78.65% of MO dye was degraded with the presence of synthesised photocatalyst within 2 hours	[51]
$CoFe_2O_4$/ rGO	Co-precipitation	Methylene blue, Rhodamine B, Methyl orange	The CoFe2O4/rGO nanocomposite material degraded MB more efficiently than MO and RhB dyes (89%, 64%, and 58%, respectively).	[52]
MoO3/ $CoFe_2O_4$	Co-precipitation	Methylene blue, Rhodamine B, Crystal violet	Almost 91 % degradation of the MB, 54% degradation of RhB and 65% degradation of crystal violet was observed by the as-synthesized nanocomposite	[53]
$CoFe_2O_4$	Microwave assisted wet chemistry method	Congo red, 4-Nitrophenol	The addition of CoFe2O4 photocatalyst exhibits improved photocatalytic activity for degradation of Congo red (96%) and 4-N (63%)	[54]
$CoFe_2O_4$	Sol-gel method	Reactive red 195	The cobalt ferrite on Reactive Red 195 (RR195) shows 74% deterioration in less than 2 hours	[55]
Al doped $CoFe_2O_4$	Solvothermal method	Methylene blue	The 93% methylene blue dye was degraded by $Co_{0.1}Al_{0.03}Fe_{0.17}O_{0.4}$ within 120 min	[56]
$CoFe_2O_4$	Chemical precipitation	Methylene blue	Achieved 99.75% photo Fenton-like degradation of MB in the presence of CoFe2 O4	[57]
Nd doped $CoFe_2O_4$	Sol-gel method	Methylene blue	The 5% Nd doping to $CoFe_2O_4$ enhanced the degradation performance of $CoFe_2O_4$	This work

Table 2: Kinetic parameters and efficiency of photocatalytic degradation of methylene blue with synthesized photocatalysts.

Photocatalyst	The rate constant (k) ($hour^{-1}$)	Correlation coefficient (R^2)	Degrading efficiency (%)
$CoFe_2O_4$	0.2828	0.996	67
5% Nd:$CoFe_2O_4$	0.3243	0.998	72
10% Nd:$CoFe_2O_4$	0.2820	0.995	69
15% Nd:$CoFe_2O_4$	0.2298	0.997	61